AIAA Meeting Papers on Disc, January 1997
A9715810, F49620-94-1-0019, F49620-95-1-0405, AIAA Paper 97-0803

Semi-implicit Runge-Kutta schemes for stiff multi-dimensional reacting flows

Jack J.-I. Yoh
California Univ., Los Angeles

Xiaolin Zhong
California Univ., Los Angeles

AIAA, Aerospace Sciences Meeting & Exhibit, 35th, Reno, NV, Jan. 6-9, 1997

This work simulates multidimensional detonation waves using the high-order Rosenbrock semi-implicit Runge-Kutta time-stepping scheme (SIRK-3C) and quantitatively compares the performance of SIRK with the second-order time-splitting schemes in dealing with the hyperbolic conservation laws with stiff relaxation terms. In the simulation of 2D detonations, a full set of elementary hydrogen-oxygen kinetics with nine species is linear-implicitly treated, while the explicit discretization of the basic advection equations is achieved by the third-order ENO schemes. Several model problems of hyperbolic systems with stiff relaxation are considered in the comparison of the time-splitting and the SIRK-3C scheme. A set of low-storage SIRK(LSSIRK) schemes is derived and tested to be high-order accurate and strongly A-stable. The results show that high-order SIRK time-stepping methods are suitable for stiff reactive flow simulations like the multidimensional detonations. (Author)

SEMI-IMPLICIT RUNGE-KUTTA SCHEMES FOR STIFF MULTI-DIMENSIONAL REACTING FLOWS

Jack Jai-ick Yoh*and Xiaolin Zhong†
University of California, Los Angeles, California 90095

Abstract

Reacting flow calculations are stiff for time-stepping. Recently, Zhong derived three sets of semi-implicit Runge-Kutta(SIRK) methods for split ordinary differential equations in the form of $u' = f(u) + g(u)$, where the nonstiff term f is treated explicitly while the stiff term g is simultaneously treated implicitly. The purpose of this work is twofold: first, to simulate multi-dimensional detonation waves using the high-order Rosenbrock semi-implicit Runge-Kutta time-stepping scheme(SIRK-3C); secondly to quantitatively compare the performance of SIRK with the second-order time-splitting schemes in dealing with the hyperbolic conservation laws with stiff relaxation terms. In the simulation of two-dimensional detonations, a full set of elementary hydrogen-oxygen kinetics with nine species are linear-implicitly treated while the explicit discretization of the basic advection equations are achieved by the third-order ENO schemes. Several model problems of hyperbolic systems with stiff relaxation are considered in the comparison of the Time-Splitting and the SIRK-3C scheme. A set of low-storage SIRK(LSSIRK) schemes is derived and tested to be high-order accurate and strongly A-stable. The results show that high-order SIRK time-stepping methods are suitable for stiff reactive flow simulations like the multi-dimensional detonations.

INTRODUCTION

In the reactive flow field solutions and the combustion related problems, the existence of several non-equilibrium states impose additional difficulties in the solutions of the reactive Euler equations with stiff relaxation terms. Since the smallest time scale is introduced from the chemical reaction kinetics, the second-order time-splitting method of Strang[1] allows an independent calculation of the stiff ODE for the source term via implicit methods in one step, and an explicit high-order convective calculation in the following time steps. By "splitting" the main source of stiffness from the basic hyperbolic conservation laws, it can accomplish a robust and easy-to-implement computation of reactive flow of current interests.

Despite the second-order in time accuracy and the robustness of these methods, there are two main difficulties with the stiffness which have been minimally handled. The spurious solutions are one of the often observed phenomena, which are stable and free of oscillations, and yet may be completely incorrect.[2] Some type of resolution technique is needed to treat this known difficulties.[3][4][5][6][7] The degrading of the second-order time accuracy to the first-order is another and quite recent observation when there exist solutions with many small-scaled structures of high-degree of complication. Jin[8] has modified the Strang splitting into the second-order time-splitting methods which preserve its high-order accuracy when the considered solutions are complicated.

New third-order semi-implicit Rosenbrock type Runge-Kutta scheme, based on the original version of Zhong[9][10], is computationally efficient with the linearized source term integration, thus requiring no iterations during the implicit treatment of the stiff source term. Third-order ENO schemes discretize the convective fluxes such that both implicit and explicit terms are treated at each of the three Runge-Kutta stages. This high-order Runge-Kutta scheme(SIRK-3C) still possesses the typical under-resolved characteristics of unphysical spurious numerical results of the Time-Splitting method. However the reduction to lower order if the small relaxation time is not temporally well-resolved, is successfully removed.

Multi-dimensional Detonations

Detonation waves are multi-dimensional and unstable phenomenon in nature as demonstrated by the early experiments of Urtiew and Oppenheim[11]. Existence of the triple points[12], consisting of an incident shock, a reflecting shock and a Mach stem, is the main characteristic of the reacting region behind the propagating shock front, and these detaching triple points from the leading front further contributes to the rolling up of vortices of opposite strength. One distinctive feature of the instability process observed in experiments is the formation of regular cell structures as triple points collide as they come together in the incident shock and move away from each other in the newly formed Mach stem. Figure[13] depicts this process of triple point col-

*Graduate Student, Member AIAA

†Assistant Professor, Mechanical and Aerospace Engineering Department, Member AIAA

lision and the trace of these points will leave a regular cell-structure pattern behind the propagation path.

Stiff Conservation Laws

The complexity of the nonequilibrium gas dynamics is a major concern in modeling of the flow field in certain regimes of hypersonic aerodynamics and combustion problems, where several nonequilibrium states exist. Many researchers over the years have developed different approaches to deal with these stiff-coupled system of equations and suggested many well-known stable high order methods.[7][13][2]. Restricting our attention to the inviscid flow, we basically have the Euler equations, coupled with source terms, representing the chemistry. In its simplest form, the linear advection model equation of Yee is stated as follows:

$$u_t + f(u)_x = S(u) \tag{1}$$

with

$$S(u) = -\mu u(u-1)(u-\frac{1}{2}) \tag{2}$$

Two stable equilibria at $u = 1$ and 0 and unstable equilibrium point at $u = \frac{1}{2}$ exist. For large μ and arbitrary initial data, the solution rapidly approaches the upper equilibrium if $u(x_0, 0) > \frac{1}{2}$ and the lower equilibrium at $u(x,t) = 0$ if $u(x_0, 0) < \frac{1}{2}$.

LeVeque and Yee[2] have considered this model problem and reported the main difficulty with the stiff system; regardless of the implicit treatment of the source term and high-order treatment of the convective term via MacCormack type predictor-corrector methods with limiter, unphysical shock speed is observed. Similar behavior was reported by Colella, Majda, and Roytburd[7] on a model combustion problem. It is known that this unphysical phenomena is due to the introduction of nonequilibrium values through numerical dissipation in the advection step. In our study, we have "nearly" removed this "turning-on" of the points within the smeared discontinuity, thus causing a wrong propagating speed, by using the Harten's subcell resolution technique similar to Ref.[3].

High-Order Accurate Simulations

The goal of the present work is to perform high-order accurate reacting flow calculations and to carry out a detailed analysis on the time-stepping methods by means of considering combustion model problems. For the fast ignition type flow as the multi-dimensional detonation problems, high order numerical scheme is desirable, in order to capture small-scale shock waves and combustion fronts. In addition, a low-storage version of the current high-order semi-implicit Runge-Kutta(LSSIRK) is derived and briefly discussed in the next section.

The reflected shock tube experiments in the strong ignition regime[14][15] and the wedge induced oblique detonation with extent to its structures and induction zone[16] [17] are first replicated numerically using a detailed hydrogen-air-argon combustion mechanism, before the simulated results of the transverse detonation waves with regular cell structures are presented. Following these one and two dimensional validations, a model combustion system of Yee[2] is used in the analysis of the two time-stepping methods, namely the Strang Time-Splitting and the SIRK-3C schemes. Another prototypical model problem of hyperbolic conservation laws with stiff relaxation terms by Chen, et al.[18] is considered to show the noticeable improvements in the solutions with complicated structures when the third-order time-stepping is used instead of the Strang-Splitting or the Second-order Splitting by Jin.[8][19]

MATHEMATICAL FORMULATION

Governing Equations

The three-dimensional governing equations for inviscid compressible reacting flows in Cartesian coordinates with the nonequilibrium chemistry and vibrational energy mode are

$$\frac{\partial \mathbf{U}}{\partial t} + \frac{\partial \mathbf{F}_j}{\partial x_j} = \mathbf{W} \tag{3}$$

where

$$\mathbf{U} = \begin{bmatrix} \rho_1 \\ \vdots \\ \rho_m \\ \rho u_1 \\ \rho u_2 \\ \rho u_3 \\ e \\ e_v \end{bmatrix} \quad \mathbf{W} = \begin{bmatrix} \dot{w}_1 \\ \vdots \\ \dot{w}_m \\ 0 \\ 0 \\ 0 \\ 0 \\ \dot{w}_v \end{bmatrix} \tag{4}$$

$$\mathbf{F}_j = \begin{bmatrix} \rho_1 u_j \\ \vdots \\ \rho_m u_j \\ \rho u_1 u_j + p\delta_{1j} \\ \rho u_2 u_j + p\delta_{2j} \\ \rho u_3 u_j + p\delta_{3j} \\ (e+p)u_j \\ e_v u_j \end{bmatrix}. \tag{5}$$

The equation of state for pressure is given by the Dalton's law for a mixture of thermally perfect gases,

$$p = \rho RT = \sum_i^m \rho_i R_i T \tag{6}$$

where R_i is the species specific gas constant. The total energy is

$$e = \sum_{i=1}^m \rho_i c_{v_i} T + e_v + \rho \frac{1}{2} u_k u_k + \sum_{i=1}^m \rho_i h_i^0. \tag{7}$$

where h_i^0 is the heats of formation, and c_{vi}, the specific heat at constant volume, is equal to $3R_i/2$ and $5R_i/2$ for monatomic and diatomic, and $6R_i/2$ for other atomic species. To account for the vibrational nonequilibrium, the thermal state of the gas is described by two separate and independent temperatures. One temperature T represents the translational and rotational modes of molecular energy while the other temperature T_v represents the energy stored in the vibrational degrees of freedom of the molecules. This approach requires a separate energy equation for vibrational energy and allows an harmonic oscillator model to be used to represent the energy in the vibrational modes. It is assumed that anharmonic effects and the excitation of electronic states are not important for the flow of interest.

The total vibrational energy is defined as

$$e_v = \sum_{i=1}^{n_m} e_{vi}. \tag{8}$$

All of the n_m species are considered to be harmonic oscillators at a single vibrational temperature T_v. e_{vi} for each diatomic molecule is expressed by

$$e_{vi} = \rho_i R_i \frac{\theta_{vi}}{e^{\theta_{vi}/T_v} - 1} \tag{9}$$

where θ_{vi} is the characteristic vibrational temperature for the single mode of vibration. Triatomic molecule, such as H_2O, has three vibrational modes so its vibrational energy is written in the harmonic approximation as

$$e_{vi} = \rho_i R_i \left(\frac{\theta_{vi_1}}{e^{\theta_{vi_1}/T_v} - 1} + \frac{\theta_{vi_2}}{e^{\theta_{vi_2}/T_v} - 1} + \frac{\theta_{vi_3}}{e^{\theta_{vi_3}/T_v} - 1}\right), \tag{10}$$

where there is a characteristic temperature for each of the three modes. Hydrogen peroxide, H_2O_2, has six vibrational modes, so its vibrational energy is written with six terms. With the vibrational energies defined in this manner, T_v can be found iteratively.

Chemical Source Terms

All of the hydrogen-air combustion in this report occur below their maximum temperature and pressure of 3500° Kelvin and 27 atmospheres respectively. For this range, the updated GRI 1.2 Mechanism[20] is proposed by numerous researchers and tested to have similar rate coefficients as the following three well known mechanisms. Moretti's 7 species (H_2, O_2, OH, H_2O, H, O and N_2 inert) 8 reactions model[21] which has been used and modified by later researchers like Cohen and Westberg, [22][23][24] is well established in the literatures and favored in the combustion work where the final equilibrium state is of prime importance. Maas-Warnatz's 9 species [25] 43 reactions add two additional species, namely HO_2 and H_2O_2. Addition of reactions involving these species is significant in the rate of relaxation of the state, including the production and consumption of species, temperature, and density. Initial testing of this mechanism revealed that the final state of the hydrogen-air combustion resulted in a close proximity to the results of 7-species model as addressed earlier. The last considered model by Oran's 9 species 48-step mechanism[15] is detailed with out the inclusion of N_2 dissociation and herein will be referred to as the "detailed model".

Of the nearly 50 reactions, the following two are the most influential in the species formation and destruction for the reasons discussed below. First and the most significant branching reaction given by

$$H + O_2 \rightleftharpoons OH + O \tag{11}$$

is the governing reaction for which radicals are created. Second type of reaction involves three-body collisions. A sample reaction is quoted from Oran's[15] as below.

$$H + OH + M \rightleftharpoons H_2O + M \tag{12}$$

which yields a reaction rate of

$$R = \sum_{i=1}^{m} \frac{\rho_i}{M_i}\left[h_i k_f \frac{\rho_H}{M_H}\frac{\rho_{OH}}{M_{OH}} - h_i k_b \frac{\rho_{H_2O}}{M_{H_2O}}\right]. \tag{13}$$

Here M refers to all possible third-body collision partners and h_i are the third-body efficiency factors for the given reaction.

Vibrational Source Term

The source terms for the vibrational equations are

$$\dot{w}_s = Q_{T-V} + Q_{V-D} \tag{14}$$

where Q_{T-V} is the translation-vibration coupling and Q_{V-D} is the vibration-dissociation coupling, following a a Landau-Teller model.[26] Although vibrational relaxation effects are small for combustion in compressing flows [27], such that the gas is essentially in thermal equilibrium, i.e. $T_v = T$, vibrational source term is considered through out the current research.

NUMERICAL FORMULATION

The governing equation(Eqn.[3]) is solved by the method of lines using a finite difference upwind scheme developed by Shu and Osher[28] to discretize the equation in space. The inviscid terms are evaluated by either ENO or TVD schemes with up to third order accuracy. As for the temporal discretization, a set of 3rd order semi-implicit Runge-Kutta(SIRK-3) schemes with three different coefficients are used in the current work. A detailed description of a spatial discretization can be found in the references [9][10] and a brief description of the semi-implicit Runge-Kutta with derived set of coefficients will be summarized below. The methods are both computationally efficient and third-order accurate

for the purpose of current two dimensional detonation simulations in this report.

There are three versions of SIRK. For SIRK-3A method,

$$\mathbf{u}^{n+1} = \mathbf{u}^n + \sum_{j=1}^{r} w_j \mathbf{k}_j \quad (15)$$

$$\mathbf{k}_i = h\mathbf{f}(\mathbf{u}^n + \sum_{j=1}^{i-1} b_{ij}\mathbf{k}_j) \quad (16)$$

$$+h\mathbf{g}(\mathbf{u}^n + \sum_{j=1}^{i-1} c_{ij}\mathbf{k}_j + a_i\mathbf{k}_i) \quad (17)$$

$$(i = 1, 2, 3) \quad (18)$$

where h is the time step ,and $\mathbf{f}$ and $\mathbf{g}$ are the results of spatial discretization of the explicit and implicit parts, respectively. All other parameters which are determined by accuracy and stability requirements are summarized in Table[1]. The computations are relatively inefficient, since nonlinear solvers, such as the Newton's method, are required to solve such nonlinear equations.

Method B and C, however require no iteration [see Zhong [9]], and they are semi-implicit extension of the Rosenbrock Runge-Kutta method,[29]

$$\mathbf{u}^{n+1} = \mathbf{u}^n + \sum_{j=1}^{r} w_j \mathbf{k}_j \quad (19)$$

$$\left[\mathbf{I} - ha_i\mathbf{J}(\mathbf{u}^n + \sum_{j=1}^{i-1} d_{ij}\mathbf{k}_j)\right]\mathbf{k}_i =$$

$$h(\mathbf{f}(\mathbf{u}^n + \sum_{j=1}^{i-1} b_{ij}\mathbf{k}_j) + \mathbf{g}(\mathbf{u}^n + \sum_{j=1}^{i-1} c_{ij}\mathbf{k}_j)) \quad (20)$$

$$(i = 1, 2, 3)$$

Here $\mathbf{J} = \frac{\partial \mathbf{g}}{\partial \mathbf{u}}$ is the Jacobian matrix of the stiff term ,and $d_{ij} = 0$ and c_{ij} for method B and C respectively. A single LU decomposition is required for these method.

Parameters	SIRK-3A	SIRK-3B	SIRK-3C
a_1	.485561	1.40316	.797097
a_2	.951130	.322295	.591381
a_3	.189208	.315342	.134705
c_{21}	.306727	1.56056	1.05893
c_{31}	.45	1/2	1/2
c_{32}	−.263111	−.696345	−.375939

Table 1: **Third-Order SIRK Methods Parameters**

$$w_1 = 1/8 \quad w_2 = 1/8$$
$$w_3 = 3/4 \quad b_{21} = 8/7$$
$$b_{31} = 71/252 \quad b_{32} = 7/36$$

Low-Storage SIRK Schemes

Work is on the progress to derive a set of high-order semi-implicit Runge-Kutta schemes which require no more than $2N$ locations. Unlike the fully implicit version of SIRK-3A which has $3N$ storage requirement, a new semi-implicit low-storage Runge-Kutta scheme(LSSIRK-3A) requires only evaluations of $\mathbf{q}_j$ and $\mathbf{x}_j$ at each of the general r-stage and takes the following form:

$$\begin{aligned} \mathbf{q}_j &= a_j\mathbf{q}_{j-1} + h[\mathbf{f}(\mathbf{x}_{j-1}) \\ &\quad +\mathbf{g}(\mathbf{x}_{j-1} + \bar{c}_j\mathbf{q}_{j-1} + c_j\mathbf{q}_j)] \\ &\quad j = 1, r \quad (21) \\ \mathbf{x}_j &= \mathbf{x}_{j-1} + b_j\mathbf{q}_j \end{aligned}$$

with $a_1 = 0$. A similar version of explicit Runge-Kutta schemes was derived by Williamson [30] and $2N$ storage version of implicit Runge-Kutta was studied by Engquist and Sjögreen[5]. However, both of these earlier derivations are not suitable for practical reactive flow calculations due to their explicit and improper treatment of the stiff source term. In the current work, proper implicit treatment of the source term $\mathbf{g}$ is enforced by searching for strictly positive implicit coefficients, c_j thus eliminating any unphysical variables which might be introduced from the negative or zero coefficients during the intermediate stages.[31]

Once 10 undetermined coefficients are written in terms of the original twelve SIRK-3A parameters, the eight accuracy conditions and one strong A-stability condition defined in Ref.[10] are used in the optimal search of the new parameters. Of the obtained four possible roots of the eight non-linear equations, additional determination criteria of a strong A-stability and large stability region defined by $c_j > 0$ further narrow down the parameter selections and the following set of new coefficients for the LSSIRK-3A is obtained:

$$c_1 = \frac{1}{5} \quad c_2 = \frac{49}{75} \quad c_3 = \frac{143}{600}$$
$$b_1 = \frac{1}{3} \quad b_2 = \frac{15}{16} \quad b_3 = \frac{8}{15}$$
$$a_2 = -\frac{5}{9} \quad a_3 = -\frac{153}{128}$$
$$\bar{c}_2 = -\frac{59}{135} \quad \bar{c}_3 = -\frac{5283}{25600}$$

Then the expressions for the third-order method become,

$$\begin{aligned} \mathbf{q}_1 &= h[\mathbf{f}(\mathbf{x}_0) + \mathbf{g}(\mathbf{x}_0 + c_1\mathbf{q}_1)] \\ \mathbf{x}_1 &= \mathbf{x}_0 + b_1\mathbf{q}_1 \\ \mathbf{q}_2 &= a_2\mathbf{q}_1 + h[\mathbf{f}(\mathbf{x}_1) + \mathbf{g}(\mathbf{x}_1 + \bar{c}_2\mathbf{q}_1 + c_2\mathbf{q}_2)] \\ \mathbf{x}_2 &= \mathbf{x}_1 + b_2\mathbf{q}_2 \end{aligned}$$

$$\begin{aligned} \mathbf{q}_3 &= a_3\mathbf{q}_2 + h[\mathbf{f}(\mathbf{x}_2) + \mathbf{g}(\mathbf{x}_2 + \bar{c}_3\mathbf{q}_2 + c_3\mathbf{q}_3)] \\ \mathbf{x}_3 &= \mathbf{x}_2 + b_3\mathbf{q}_3 \end{aligned} \quad (22)$$

These obtained coefficients have been tested to hold their third-order accuracy. Moreover, complete discussions of all three low-storage versions of semi-implicit Runge-Kutta schemes of up to four stages with extension to the non-autonomous version[32] will be reported in the forthcoming paper.

RESULTS with DETAILED CHEMISTRY

The new third order semi-implicit Runge-Kutta code(SIRK-3C) was tested with one-dimensional reflected reacting shock tube experiment before it was applied to two-dimensional detonation cases. In the first case of strong ignition shock reflection, $H_2 - O_2 - Ar$ mixture is used. Following Cambier[16] and Li[17], we then conducted two dimensional wedge induced oblique detonation simulations with N_2 as an inert gas instead of Ar.

Reflected Shock Tube

Detailed ignition processes in hydrogen-oxygen-argon mixtures behind a shock wave reflected from a rigid wall are simulated, based on the shock tube experiments performed by Cohen and Larsen[14]. The corresponding numerical simulation is carried out by Oran, et al.[15] who use the Flux Corrected Transport(FCT) method along with an adaptive grid in their solutions.

We used the detailed 48-step chemical reaction with 9 species as discussed earlier, which is the identical combustion mechanism used in the simulation of Oran, et al. [15] Figure[1] represents the schematic of the shock tube, where incident shock is reflected and then followed by a reacting shock. The initial mixture of the gases is $2H_2 + 1O_2 + 7Ar$. Only a slight difference in the initial conditions to the experiment is observed and summarized in Table[2].

	Undisturbed	Incident	Reflected
T	298.0°K	621.0°K	1036°K
P	6687.45Pa	36670.6Pa	131722.5Pa
u_{Fluid}		465.4m/s	
u_{Shock}		756.1m/s	450m/s

Table 2: **Parameters for the Strong Ignition Simulation**

A coarse grid of 100 cells with uniform spacing($\Delta x = 0.12cm$)is used, and the results agree well with both finer grid case($\Delta x = 0.035cm$) of Oran, et al. and experiment of Cohen. Figure[2] shows a combined x-t plot of all the cases considered here. Relative to the point at which the transmitted detonation forms (approximately at $t = 260\mu$sec), two additional snap shots are taken such that before and after behavior of reflected shock-reacting shock and transmitted detonation-contact discontinuity structure are considered. Figure[3] and Figure[4] show a good agreement with the reported results[15] and in particular reflected expansion wave is reasonably well observed even at our coarse grid result as in Figure[4].

Before moving on to the multi-dimensional simulation, we applied different sets of rate coefficients suggested by Moretti and Maas-Warnatz and found that similar structures are obtained but clearly different ignition delay was observed. It is believed that the discrepancy in the magnitudes of the main branching reaction rate coefficients(see Eqn.[11]) causes this ignition time difference and thus for this simulation, choice of Oran's full mechanism was a crucial factor in achieving such well-agreeing results.

Wedge-Induced Detonation

Computational domain used in the two-dimensional wedge detonation problem is sketched in Figure[5]. So, for a simulation of supersonic premixed fuel hitting the wedge at an angle θ, incoming flow at the left boundary is at this angle to the domain such that a uniform grid can be used.

Standing Oblique Detonation with Fast Ignition

The revisited test case of the two dimensional oblique detonation problem is Cambier, Adelman and Menees.[16] The free stream conditions are as in Table[3]. The dimensions of the system is $28cm$ by

Case	M_∞	T_∞	P_∞,atm
2	3.8	840	0.0600

Table 3: **Freestream Conditions for $H_2 : O_2 : N_2/0.201 : 0.168 : 0.631$ by Mass**

$10cm$ and 50 and 75 points are used in the x and y direction. The mixture of 60% stoichiometry and chosen initial conditions can ignite the fuel instantaneously and thus coupled shock and detonation are observed on a wedge of 31^o degrees.(see Figure[6]) The ignition temperature of the mixture is around 1000°Kelvin, so that high freestream temperature drives the shock-detonation coupling at a supersonic speed of 3.8. Figure[7] and Figure[8] show temperature and pressure distribution along the cut at grid row 32. Slightly different cut was chosen in Cambier's results[16], but reasonably identical profiles were obtained in our simulation. Discrepancy in the rate of relaxation of temperature is believed to come from the omission of three elementary reaction steps from the detailed model by the authors Cambier, Adelman and Menees. A major reason for their removal of several steps was due to errors

during the process of manuscripting the compiled reactions reported in the reference.[15] For our detonation code, corrected and accurate version of this mechanism is implemented with several personal acknowledgments from authors.

Standing Oblique Detonation with Induction

A different set of initial conditions to that of the previous shock induced detonation simulation is listed in Table[4] and it corresponds to the case reported in Li, Kailasanath, and Oran.[17]

Wedge angle	M_∞	T_∞	P_∞,atm
23^o	8.0	300°K	1.0

Table 4: **Freestream Conditions**

The size of the computational domain is $10.0cm$ x $3.5cm$ and the numerical resolution is $\Delta x = \Delta y = 0.05cm$ such that 200 and 70 points are used in x and y directions respectively. All three hydrogen-air mechanisms were used to simulate this case and with its most detailed nature, Oran's full mechanism results are included in this report.

For the given conditions, non-reacting post shock state has been analyzed and compare well with the obtained results as in Table[5]. Figure[9] and Figure[10]

	Non-reacting aftershock state
Temperature	1300^o Kelvin
Pressure	1900kPa
Mach Number	3.5

Table 5: **Behind Non-reacting Shock Conditions**

are the reacting cases with initial species molar concentration of $H_2 : O_2 : N_2$ / 2 : 1 : 3.76. While only a small induction zone is obtained in the simulation, the final or the equilibrium state values for temperature and pressure down stream of the detonation structure report in good agreement with results by Li, et al.[17] Figure[11] basically addresses these agreements by presenting profiles of temperature, pressure,Mach number, and mass fraction of H_2O product along the x direction at $1mm$ above the wall.

While obtaining a very stable and fast reacting combustion front results, we then slightly varied the initial species concentration which will result in an induction zone behind an oblique shock. $H_2 : O_2 : N_2$ composition of 0.296 : 0.148 : 0.556 by mass was used to generate a structure of oblique detonations, consisting of a non-reactive oblique shock, and induction region, a set of deflagration waves, and a detonation front. Figure[12] depicts this structure and suggests grid refining for resolving the near wall behavior of the deflagration waves.

The numerical code(FCT) used in the work of Li, et al. is second order in space and second order in time, while keeping the chemistry part simplest via the induction parameter model.[33] In the current simulation, 48-step combustion mechanism was considered and third order accuracy in time and space was achieved. Reported discrepancies in the induction zone structure is under continued investigation and full description of the explanations and suggestions will be reported in the future.

RESULTS of MULTI-DIMENSIONAL DETONATION WAVES

Basic Equations

Reactant is converted to product by a single-step irreversible chemical reaction, governed by Arrhenius kinetics. The specific heat ratio, γ is fixed at 1.2, and a dimensionless parameter, Q^+ is also introduced for the specific heat of formation. The specific total energy is

$$\frac{e}{\rho} = \frac{p}{\rho(\gamma-1)} + \frac{u^2+v^2}{2} + Q^+ Z R T_0 \qquad (23)$$

where Z is used to represent the reactant mass fraction, namely the ratio of ρ_1 to ρ total. Further T_0 is the unreacted flow temperature. From this type of formulation of total energy, the temperature can be obtained by replacing p/ρ with RT such that the temperature T can be solved once all other values are computed from the numerical conservative value, e. Further, the case of one-step $R \rightarrow P$ irreversible reaction can be represented by the Arrhenius kinetics such that

$$\dot{w}_1 = -\mathbf{K}\rho_1 e^{\frac{-E^+ T_0}{T}} \qquad (24)$$

$$\dot{w}_2 = 0 \qquad (25)$$

Here, E^+ is the activation energy parameter and T_0 is again the initial temperature of the unreacted gas mixture.

Initial Setup

The initial data consist of the theoretical Z-N-D profiles on which a transverse perturbation must be added to excite a fully multi-dimensional instability. If no transverse gradient is present in the initial data, one-dimensional profile will be preserved such that only a longitudinal instability, if it exists, can be observed. A small sinusoidal perturbation of the form, $u = u + \epsilon u \sin(8\pi y)$ is prescribed on the front of the wave and each fluid variables in the Chapman-Jouguet states can also be perturbed in a similar manner. The following is a description of the Chapman-Jouguet states used as the initial data in the present simulation. The overdrive parameter f, which is defined as the square of

	Burnt(Postshock)	**Unburnt**(Preshock)
T	$T_{CJ} = 2853°K$	$298°K$
P	$P_{CJ} = 116,717Pa$	$6666Pa$
u	$D = 1956.46m/s$	0
γ	1.2	1.2
M_{shock}	1.095	

Table 6: **Flow Conditions with Chapman-Jouguet States**

the ratio of the detonation propagation velocity to the Chapman-Jouguet velocity, $f = (D/D_{CJ})^2$, is held at 1.2. Erpenbeck[34] gives one possible form for this C-J detonation speed:

$$D_{CJ} = \sqrt{\frac{1+Q^+(\gamma^2-1)}{2\gamma}} + \sqrt{\frac{Q^+(\gamma^2-1)}{2\gamma}} \qquad (26)$$

where Q^+ is also a known parameter such that the initial inflow speed D can be set accordingly.

Two-Dimensional Detonation Waves with Regular Cell Structures

M-type Z-N-D waves are perturbed to develop into two-dimensional detonation waves with regular cell structures using the third-order semi-implicit Runge-Kutta scheme for highly accurate time stepping and the third-order ENO schemes for high-order shock capturing calculations. A set of uniform 300 by 300 grids was used in the physical domain of a 9 by 9cm duct using periodic boundary conditions in the transverse direction. The data for this case are given below:

γ	E^+	Q^+	f	L_x	L_y
1.2	10	50	1.2	9cm	9cm

Table 7: **Parameters Used in the Simulation**

For the mixture of ideal gas with constant $\gamma = 1.2$, molecular weight, and heat of reaction, the chemistry is modeled with a single-step reaction governed by Arrhenius kinetics. The reaction coefficient **K** in Eqn.[24] is chosen at 3.124. Figure[14] depicts the evolving Mach structures and triple-point collisions from which one can see the rolling up of the vortex sheets as soon as they detach from the triple points at the detonation front.

Coarse Grid	**Fine Grid**
300 x 300	600 x 600

Table 8: **Computational Domain Size**

The converged results are assured by the continuing reproduction of the vortex pairs. At a qualitative level, maximum vorticity peak to peak distances ratios are measured and compared within 6% of error to the reported results of Bourlioux[35]. Figure[15] is a sequence of density contours in which the regular cell pattern behind the detonation front is observed, and the similarity in the mushroom like vortex structures to the reported results of Bourlioux is further obtained. Furthermore, the grid independence check was performed by running a similar condition at a 600 by 600 grid size, and the obtained vorticity contour in Figure[16] reports no additional structures to that of the coarse grid cases at 300 by 300. Calculated paths of triple point movements in Figure[17] is a representation of an approximate measure of the cell size and the cell reproduction time. It is a y-t contour plot of pressure from which one can estimate the cell size corresponding to species of the given idealized system. A typical one-cell size of hydrogen-air detonation is of order $10(\mu sec)$[36] and the observed size in the current simulation is approximately $38(\mu sec)$.

Since the simulation of an idealized multi-dimensional detonation involving an one-step irreversible chemical reaction with two species present is valid only at a qualitative level, a detailed $H_2 - O_2$ mechanism was also implemented in the further computation and validation of detonation waves with all of the nonequilibrium effects as considered in previous one-dimensional test cases. Table[9] lists the flow conditions of the multi-species, thermal and chemical nonequilibrium flow simulation performed here.

	Burnt(Postshock)	**Unburnt**(Preshock)
T	$2300°K$	$298°K$
P	$304,000Pa$	$6666Pa$
u	$1618m/s$	0
γ	1.556	1.556

Table 9: **Flow Conditions for a Computation with Detailed Model of Chemical Kinetics and Thermophysics for $H_2 : O_2 : Ar/2 : 1 : 7$ Two-Dimensional Detonation**

A good agreement with both experiment (Dormal, Libouton & Van Tiggelen 1979[37]) and numerical simulation(Lefebvre, Kailasanath & Tiggelen 1993[36]) is obtained for a well shaped cellular pattern characteristic of detonations in argon-diluted, low-pressure mixtures of hydrogen and oxygen. 156 grids span a channel of width $4.68cm$ and one-dimensional reacting shock is initially perturbed to develop into unstable transverse detonation waves. The observed triple point movement coincides with the reported results of Lefebvre and Oran, and computed cell size is also identical as in the experiment. Only a small discrepancy is noted in the computed average detonation speed(see Table[10]) , where the speeds 1640, 1623, 1475, and 1619 m/s correspond

to the values obtained from SIRK-3C, the computed value of Lefebvre[36], the experimental value of Dormal, Libouton and Van Tiggelen(1979)[37], and the calculated CJ detonation velocity[36] , respectively.

	D_{ave}(m/s)
SIRK-3C	1640
Numerical Simulation by Lefebvre	1623
Experiment by Dormal, et al.	1475
C-J velocity	1619

Table 10: **Comparison of Computed Average Detonation Velocity, D_{ave}, to the Previously Reported Values**

All of the significant structures of the detonation region is observed including the continuous evolution of Mach structure with spinning contact discontinuity. Observations regarding the $H_2 - O_2$ detonation waves are intended for suggesting the ball-point average speed of the propagating detonation waves in a combustible mixture, and further supports the time accuracy nature of the high-order semi-implicit Rosenbrock Runge-Kutta(SIRK-3C) scheme.

STIFF RELAXATION SYSTEMS

The high order Semi-Implicit Rosenbrock Runge-Kutta schemes have been tested in multi-dimensional detonation cases and shown to reproduce previously reported results of both numerical simulations and experiments. Work is continued on the comparison of the SIRK-3C scheme to the Strang Time Splitting methods in stiff model problems of Yee[2] and Chen, et al.[18] for a discontinuity and a smooth sinusoidal wave propagation.

Semi-Implicit Coupling vs. Time-Splitting

In going about the solving of the fluid and stiff source terms, one can achieve a second order in time integration by the time-splitting or the fractional stepping[38][39]. Applying the Strang splitting[1] to maintain the second order accuracy, the solution at time $n+1$ is given as

$$u^{n+1} = \mathcal{L}_S(k/2)\mathcal{L}_f(k)\mathcal{L}_S(k/2)u^n \tag{27}$$

where each fluid and reaction operators are denoted $\mathcal{L}_f$ and $\mathcal{L}_S$ respectively. A half step in time is taken in the linear implicit solving of the source term and the solution is used as an initial value to solve a full one step fluid calculation. Final half step in time is taken in updating the source term calculation achieving efficiently second order in time, and spatial accuracy is determined arbitrarily depending on the choice of a convective scheme by the user. Here we described the exact version that is used in the present analysis of time stepping schemes and thus ENO-Roe-S-3(see Shu and Osher[28]) scheme is used in calculating the inviscid flux term, further advanced in time via explicit RK-3. This allows the flux operator $\mathcal{L}_S(k)$ locally third order in time and third order in space.

$$\begin{aligned}
\mathcal{L}_S(k/2): \quad & [1 - \tfrac{1}{4}kS'(u_j^n)]\Delta u_j^* = \tfrac{1}{2}kS(u_j^n) \\
& u_j^* = u_j^n + \Delta u_j^* \\
\mathcal{L}_f(k): \quad & K_1 = -\tfrac{k}{h}F(u_j^*) \\
& K_2 = -\tfrac{k}{h}F(u_j^* + b_{21}K_1) \\
& K_3 = -\tfrac{k}{h}F(u_j^* + b_{31}K_1 + b_{32}K_2) \\
& u_j^{**} = u_j^* + \omega_1 K_1 + \omega_2 K_2 + \omega_3 K_3 \\
\mathcal{L}_S(k/2): \quad & [1 - \tfrac{1}{4}kS'(u_j^{**})]\Delta u_j^{**} = \tfrac{1}{2}kS(u_j^{**}) \\
& u_j^{n+1} = u_j^{**} + \Delta u_j^{**}
\end{aligned} \tag{28}$$

In achieving a high order in space, the convective flux discretization of Shu and Osher was used.[28]

SIRK-3C treats the flux discretization $F(u)$ explicitly and the source term $S(u)$ implicitly via semi-implicit fashion. A scalar version in relevance to the current time-stepping analysis is written as follows:

$$K_1 = \frac{-\frac{k}{h}F(u_j^n) + kS(u_j^n)}{1 - ka_1S'(u_j^n)} \tag{29}$$

$$K_2 = \frac{-\frac{k}{h}F(u_j^n + b_{21}K_1) + kS(u_j^n + c_{21}K_1)}{1 - ka_1S'(u_j^n + c_{21}K_1)} \tag{30}$$

$$K_3 = \frac{[-\frac{k}{h}F(u_j^n + b_{31}K_1 + b_{32}K_2) + kS(u_j^n + c_{31}K_1 + c_{32}K_2)]}{1 - ka_1S'(u_j^n + c_{31}K_1) + c_{32}K_2} \tag{31}$$

$$u_j^{n+1} = u_j^n + \omega_1 K_1 + \omega_2 K_2 + \omega_3 K_3 \tag{32}$$

where in this scalar format, the Jacobian J is replaced by the derivative, $S'(u)$, and all of the Runge-Kutta coefficients were reported in the earlier work. Here, $F(u)$ is discretized in the same fashion as in the Time-Splitting case and thus third order ENO-Roe is again implemented. Another version of the SIRK, namely the fully iterative SIRK-3A, was also implemented in the current analysis and the code performances to the time-split approach is reported herein.

Propagation of a Discontinuity

When the initial condition is given by the piecewise constant data,

$$u(x,0) = \begin{cases} 1 & \text{if } x < 0.3 \\ 0 & \text{if } x > 0.3 \end{cases} \quad (33)$$

and the stiffness parameter $k\mu$ is much larger than 1, the solution is a propagating step function at incorrect speeds. This stiffness parameter is called the "cell Damköhler number", which is a ratio of advection time scale Δt to the relaxation time scale for the source term, namely $\frac{1}{\mu}$. Figure[18] shows the result of solving this model equation with Time-Splitting/ENO-Roe-3/RK-3, and SIRK-3C/ENO-Roe-3 schemes.

Two methods become nearly identical when stiffness is reduced to zero as in the case $k\mu = 0$. This adds to the observation that approximately one cell is used to capture a shock after the subcell resolution at the ENO convective stage. When the stiffness is large such that the cell Damköhler number becomes much greater than 1, the prediction of the shock location starts to fail. In fact at a very highest stiffness at $k\mu \geq 15$, the discontinuity does not propagate at all. This is understood as the small time scale introduced from the source term relaxation governs the computation, thus the points within the discontinuity are turned on incorrectly. We have also shown that this improper excitation of the points within the discontinuity has even a greater effect in the overall stiffness test when the original ENO-3 without the subcell resolution or the basic TVD is used instead.

Chang[4] has applied the idea of subcell resolution technique on the source term calculation in addition to applying it at the ENO stage, and have shown to improve the range of stiffness at which the shock location is correctly predicted. For our analysis, we have shown a slight improvement of predicting the propagating discontinuity speeds to the original results of LeVeque and Yee and further implemented a higher order in time and more sophisticated ENO-3 convective schemes to show that both SIRK-3C and Time-Splitting methods fail when a large stiffness is encounted. A fully iterative SIRK-3A is also tested against this model problem and found to produce similar results as the SIRK-3C.(see Figure[19]) This expected phenomenon motivates us to conduct a detailed analysis of the two methods of other kinds while allowing only a fixed stiffness that will allow a thorough temporal as well as spatial accuracy comparison. The propagation of an initially smooth sinusoidal data is discussed in the following section.

Propagation of a Smooth Function

The model equation of non-homogeneous hyperbolic equation have three points of equilibria as mentioned earlier. When the unstable points other than the three points are used as the initial condition, the solution tends to either the two of the stable equilibria, namely 0 or 1. Following the linear perturbation analysis, one can approximate an exact solution to the system. Let u is described by one of the following three expressions, and apply these to the system as initial data:

$$u = 1 + \varepsilon u' \quad (34)$$

$$u = 0 + \varepsilon u' \quad (35)$$

$$u = \frac{1}{2} + \varepsilon u' \quad (36)$$

while the perturbation parameter ε is kept small (usually less than 10^{-3}) in order for the linear perturbation analysis to hold true. Also u' is a derivative of u with respect to t. If we let $u = 1 + \varepsilon u'$ as initial data, the governing equation with an order of magnitude analysis can become:

$$u'_t + u'_x = -\mu \frac{u'}{2} \quad (37)$$

where the fluctuation magnitude, $A(t)$, can be solved for. The expression for $u' = A(t)e^{i\alpha x}$ is substituted, and then found $A(t) = e^{[\frac{\mu}{2} + i\alpha]t}$. For a small value of ε, the analytical solution is finally obtained:

$$u(x,t) = 1 + \varepsilon e^{-\frac{\mu}{2}t} e^{i\alpha(x-t)} \quad (38)$$

Similar analysis can be done to find solutions to the two other points of equilibrium as well.

Figure[20] depicts the numerical solution of the system at time 0.09375 when $u = 1 + \varepsilon \cos \alpha x$ is used as initial data. In order to minimize spatial error accumulation from the current TVD or ENO scheme, we have derived the following explicit upwind scheme of order three:

$$\frac{\partial f(u)_j}{\partial x} = \frac{f(u)_{j-2} - 6f(u)_{j-1} + 3f(u)_j + 2f(u)_{j+1}}{6\Delta x} \quad (39)$$

Periodic conditions are enforced on the boundaries of a single wave domain of length and period of a unity. A convenient parameter of the system stiffness, the "Damköhler number $\mathcal{D}$" is defined as the ratio of the fluid time scale to the reaction time scale. A period of 1 is taken as the fluid time scale, while $\frac{2}{\mu}$ is the representative reaction time scale.

$$\mathcal{D} = \frac{t_{fluid}}{t_{reaction}} = \frac{1}{\frac{2}{\mu}} \quad (40)$$

For the solution in the figure, this Damköhler number and the CFL number are kept at 30 and 0.75 respectively, allowing relatively large Δt for the time advancement.

Table[11] briefly summarizes the L_∞ norm error, defined by $L_\infty = max|u_i - u_{i_{exact}}|$. The error ratios R_3 for SIRK-3C and R_2 for Time-Splitting show that the schemes are pth-order accurate in time. That is the computed error ratios when the Δt is halved to $\frac{\Delta t}{2}$, should become $R_3 = 2^3 = 8$ and $R_2 = 2^2 = 4$, as

CASE	SIRK-3C		TIME-SPLIT	
	L_∞	R_3	L_∞	R_2
Δt	0.178x10^{-8}		0.108x10^{-7}	
$\frac{\Delta t}{2}$	0.221x10^{-9}	8.05	0.248x10^{-8}	4.37

Table 11: **Numerical Errors with $\mathcal{D} = 30$ and $\lambda = 0.75$**

clearly it is the case in the reported results. With the magnitude of L_∞ norm error nearly 11 times greater than that of the SIRK-3C, Time-Splitting scheme has its errors mainly evolved from the temporal accuracy. This is an expected behavior of a second-order scheme that when Δx is reasonably small, the effect of temporal accuracy is significant in total error, suggesting a higher order scheme like the SIRK-3C.

When the solution does not evolve it self with many small scale structures and thus a fast and efficient method is simply needed to do the job, the time-splitting is the way to go. As shown in this paper and others, time-splitting can meet most of the stiffness features of the problem. Nevertheless, when introduced a complicated flow structures with presence of many small scale structures, like the small rolling up of the vorticies and the triple point structures behind a propagating two-dimensional detonation, SIRK-3C can be more appropriate. Although the users must compromise between the robustness at a very high stiffness and the accuracy at a reasonably high stiffness, when going about choosing one of the two considered time-stepping methods in this paper.

Navier-Stokes Limit Model

A prototypical relaxation model[18] is now considered to suggest the reduced accuracy of the Splitting schemes for a solution with complicated structures.

$$\partial_t h + \quad \partial_x w \quad = 0 \tag{41}$$

$$\partial_t w + \quad \partial_x (h + \tfrac{1}{2}h^2) \quad = -10^8 (w - \frac{1}{2}h^2) \tag{42}$$

with initial conditions

$$h(x,0) = \quad 1 + 0.2\sin(8\pi x) \tag{43}$$

$$w(x,0) = \quad \tfrac{1}{2}h(x,0)^2 \tag{44}$$

This is a 2x2 system with its long-time behavior analogous to a parabolic system with added convection term as noted below:

$$w = \quad \tfrac{1}{2}h^2 - 10^{-8}(1 + h - h^2)\partial_x h, \tag{45}$$

$$\partial_t h + \partial_x (\frac{1}{2}h^2) = \quad 10^{-8}\partial_x[(1 + h - h^2)\partial_x h]. \tag{46}$$

The "Damköhler number" as in the previous cases is 10^8, making the considered problem a hyperbolic system with relaxation terms at its limit of stiffness. The spatial resolution is fixed at $\Delta x = 10^{-2}$ while the temporal increment is chosen at $\Delta t = 0.005$. At time $t = 0.3$, numerical solutions are obtained for both the Strang-Splitting and SIRK-3C time stepping methods and illustrated in Figure[21]. Shi Jin has considered the same problem and have shown to improve the typical first order behavior of the Strang Splitting for complicated structured solutions by the second-order time splitting.[8] This second-order time-splitting takes the following form and it basically combines the two-stage explicit Runge-Kutta and the stiff ODE solver:

$$\begin{aligned}
\mathcal{L}_s(a\Delta t): \quad \mathbf{u}^* &= \mathbf{u}^n + a\Delta t s(\mathbf{u}^*) \\
\mathcal{L}_f(\Delta t): \quad \mathbf{u}^{(1)} &= \mathbf{u}^* - \frac{\Delta t}{\Delta x}\mathbf{f}(\mathbf{u}^*) \\
\mathcal{L}_s(b\Delta t, c\Delta t): \quad \mathbf{u}^{**} &= \mathbf{u}^{(1)} + b\Delta t s(\mathbf{u}^{**}) \\
&\quad + c\Delta t s(\mathbf{u}^*) \\
\mathcal{L}_f(\Delta t): \quad \mathbf{u}^{(2)} &= \mathbf{u}^{**} - \frac{\Delta t}{\Delta x}\mathbf{f}(\mathbf{u}^{**}) \\
\mathbf{u}^{n+1} &= \frac{1}{2}(\mathbf{u}^n + \mathbf{u}^{(2)})
\end{aligned} \tag{47}$$

The method is second order if the coefficients are chosen as follows[8]:

$$a = -1, b = 1, c = 2$$

The convective operators, $\mathcal{L}_f$ combine to give the second-order explicit Runge-Kutta method when the source term is zero.($\mathbf{s}(\mathbf{u}) = 0$)

In order to reduce any additional errors introduced from the spatial calculations and thus to make a fair comparison of the three time stepping methods, two additional cares are considered:

(a) For the system of two variables, flux-vector splitting is used based on the two characteristic wave speeds, namely $\pm\sqrt{1+h}$.

$$\frac{\partial \mathbf{u}}{\partial t} + \mathbf{A}^+\frac{\partial \mathbf{u}}{\partial x} + \mathbf{A}^-\frac{\partial \mathbf{u}}{\partial x} = 0 \tag{48}$$

where the Jacobian matrices $\frac{\partial \mathbf{f}}{\partial \mathbf{u}}$ or $\mathbf{A}^+$ and $\mathbf{A}^-$ are given by,

$$\mathbf{A}^+ = \frac{1}{2}\begin{bmatrix} \sqrt{1+h} & 1 \\ 1+h & \sqrt{1+h} \end{bmatrix} \tag{49}$$

$$\mathbf{A}^- = \frac{1}{2}\begin{bmatrix} -\sqrt{1+h} & 1 \\ 1+h & -\sqrt{1+h} \end{bmatrix} \tag{50}$$

Here the matrix T is the eigen vector matrix for the two eigen values, and the vector $\mathbf{u}$ is given by $\mathbf{u} = [h, w]^T$. Depending on the direction of the characteristic waves,

one of the following third-order explicit upwind schemes are used:

$$\left.\frac{\partial \mathbf{u}}{\partial x}\right|_{\lambda+} = \frac{\mathbf{u}_{j-2} - 6\mathbf{u}_{j-1} + 3\mathbf{u}_j + 2\mathbf{u}_{j+1}}{6\Delta x} \qquad (51)$$

$$\left.\frac{\partial \mathbf{u}}{\partial x}\right|_{\lambda-} = \frac{-\mathbf{u}_{j+2} + 6\mathbf{u}_{j+1} - 3\mathbf{u}_j - 2\mathbf{u}_{j-1}}{6\Delta x} \qquad (52)$$

(b)For both of the time-splitting schemes, the stiff ODEs or the chemical relaxation equations are solved with the Newton's iteration method in order to "eliminate" any additional errors from solving them approximately. Noticeable improvement in the solution is obtained from this second-order time-splitting of Shi Jin; however, the solutions still overshoot at the locations of complicated structures and thus illustrate an inferior result to those of the SIRK-3C. It is fairly appropriate to say that both of the Strang Time-Splitting and the improved Second-Order Splitting fail to approximate the exact solutions with complicated structures as accurately as the third-order Semi-Implicit Rosenbrock Runge-Kutta scheme, and the high-order temporal calculation is a critical parameter when considering a stiff relaxation system with existing small scale structures as in many of the reactive flow situations, considered in this paper. Figures[22 - 24] also support the same observations at a varied range of stiffness.

CONCLUDING REMARKS

New high-order semi-implicit Runge-Kutta schemes are applied to simulate multi-dimensional detonation waves with complicated small scale structures. Unlike the conventional second-order time-splitting methods, these new time-stepping methods preserve their third-order accuracy even if the small relaxation time is not temporally well-resolved. Because of the coupling between the source and fluid terms in each of the Runge-Kutta stages, SIRK-3C may become less robust than the decoupled time-splitting methods when the under-resolved chemical relaxation time scale approaches its limit at zero. However, numerical analyses of this paper and others have shown the generation of totally incorrect and yet stable results at this theoretical limit of stiffness. Then how one can compromise between the high-accuracy of the solutions over the robustness of the code at the stiffness limit will depend on the applications on which the proposed schemes will be considered. In conclusion, as far as the multi-dimensional detonation waves are concerned, either time-stepping methods with the third-order convective schemes with some type of resolution technique will be suitable for a fairly accurate results; however, for added confidence in the obtained numerical results, second-order time-splitting should be used if the imposed chemical relaxation time scale due to a considering combustion mechanism is considerably close to the asymptotic limit of stiffness; however, the semi-implicit Runge-Kutta scheme has discernible advantages over the time-splitting when small scale structures are evident in the solutions.

ACKNOWLEDGMENTS

This research was partly supported by the Air Force Office of Scientific Research under grant numbers F49620-94-1-0019 and F49620-95-1-0405 monitored by Dr. Len Sakell. More information on this work and related on-going research can be found on the World Wide Web at http://CFDLAB5.seas.ucla.edu.

References

[1] G. Strang. On the Construction and Comparison of Difference Schemes. *SIAM J. Numer. Anal.*, 5:506–517, 1968.

[2] R.J.LeVeque and H.C.Yee. A Study of Numerical Methods for Hyperbolic Conservation Laws with Stiff Source Terms. *Journal of Computational Physics*, 86:187–210, 1990.

[3] A.Harten. High Resolution Schemes for Hyperbolic Conservation Laws. *Journal of Computational Physics*, 49:357–393, 1983.

[4] Shih-Hung Chang. On the Application of Subcell Resolution to Conservation Laws with Stiff Source Terms. *NASA TM-102384*, pages 1–12, 1989.

[5] B.E.Engquist and B. Sjögreen. Robust Difference Approximations of Stiff Inviscid Detonation Waves. *UCLA CAM Report 91-03*, 1991.

[6] Eduard Harabetian. A Subcell Resolution Method for Viscous Systems of Conservation Laws. *Journal of Computational Physics*, 103:350–358, 1992.

[7] P.Colella, A.Majda, and V.Roytburd. Theoretical and Numerical Structure for Reacting Shock Waves. *SIAM J. Sci.Stat.Comput.*, 7:1059–1080, 1986.

[8] Shi Jin. Runge-Kutta Methods for Hyperbolic Conservation Laws with Stiff Relaxation Terms. *Journal of Computational Physics*, 122:51–67, 1995.

[9] Xiaolin Zhong. New High-Order Semi-Implicit Runge-Kutta Schemes for Computing Transient Nonequilibrium Hypersonic Flow. *AIAA Paper 95-2007*, pages 397–407, 1995.

[10] Xiaolin Zhong. Additive Semi-implicit Runge-Kutta Methods for Computing High-Speed Nonequilibrium Reactive Flows. *Journal of Computational Physics*, 128:19–31, 1996.

[11] P.A.Urtiew and A.K.Oppenheim. Experimental Observations of the Transition to Detonation in an Explosive Gas. *A Proc.Roy.Soc.London*, 295:13–28, 1966.

[12] W.Fickett and W.C.Davis. *Detonation*. University of California Press, Berkeley, 1979.

[13] P.Colella and P. Woodward. The Piecewise Parabolic Method (PPM) for Gas-Dynamical Simulations. *Journal of Computational Physics*, 54:174–201, 1984.

[14] A.Cohen and J.Larsen. *Acta Astronautica*. B.R.L. Report No.1386, Aberdeen, Maryland, 1967.

[15] E.S.Oran, T.R.Young, J.P.Boris, and A.Cohen. Weak and Strong Ignition. I.Numerical Simulations of Shock Tube-Experiments. *Combustion and Flame*, 48:135–148, 1982.

[16] J. Cambier, H. Adelman, and G. P. Menees. Numerical Simulations of Oblique Detonations in Supersonic Combustion Chambers. *Journal of Propulsion*, 5:482–491, 1989.

[17] Chiping Li, K. Kailasanath, and E.S. Oran. Detonation Structures Behind Oblique Shocks. *Physics of Fluids*, 6:1600–1611, 1994.

[18] G.-Q. Chen, C.D.Levermore, and T.-P Liu. *Comm. Pure Appl. Math.*, 47:787, 1994.

[19] Shi Jin and C.D.Levermore. Numerical Schemes for Hyperbolic Conservation Laws with Stiff Relaxation Terms. *Journal of Computational Physics*, 126:449–467, 1996.

[20] CHEMKIN. *GRI 1.2 CHEMKIN*. the Gas Research Institute, 1995.

[21] Gino Moretti. A New Technique for the Numerical Analysis of Nonequilibrium Flows. *AIAA Journal*, 3:223–229, 1965.

[22] N.Cohen and K.Westberg. Chemical Kinetic Data Base for High-Temperature Chemical Reactions. *Journal of Physical and Chemical Reference Data*, 12:531–590, 1983.

[23] S.M.Dash and H.S.Pergament. *The JANNAF Standard Plume Flowfield Model*. JANNAF 12th Plume Technology Meeting, 1980.

[24] J.S.Evans and C.J.Schexnayder. Influence of Chemical Kinetics and Unmixedness on Burning in Supersonic Hydrogen Flames. *AIAA Journal*, 18:188–193, 1980.

[25] U.Maas and J.Warnatz. Ignition Processes in Hydrogen-Oxygen Mixtures. *Combustion and Flame*, 74:53–69, 1988.

[26] R.C.Millikan and D.R.White. Systematics of Vibrational Relaxation. *Journal of Chemical Physics*, 39:3209–3213, 1963.

[27] G.J.Wilson. *Computation of Steady and Unsteady Shock-Induced Combustion Over Hypervelocity Blunt Bodies, PhD Dissertation*. Stanford University, 1991.

[28] C.-W.Shu and S.Osher. Efficient Implementation of Essentially Non-oscillatory Schemes II. *Journal of Computational Physics*, 83:32–78, 1989.

[29] H.H.Rosenbrock. Some General Implicit Processes for the Numerical Solution of Differential Equations. *Comput. J.*, 5:329, 1963.

[30] J.H.Williamson. Low-Storage Runge-Kutta Schemes. *Journal of Computational Physics*, 35:48–567, 1995.

[31] Björn Sjögreen. Numerical Computation of Three Dimensional Detonation Waves on Parallel Computers. *Uppsala University Report 162-1994*, 1994.

[32] Jian-Wei Shen and Xiaolin Zhong. Semi-Implicit Runge-Kutta Schemes for Non-Autonomous Differential Equations in Reactive Flow Computations. *AIAA Paper-96-1969*, 1996.

[33] E.S.Oran, M.Picone, et al. *Numerical Simulations of Detonations in Hydrogen-Air and Methane-Air Mixtures*. The Combustion Institute, 1981.

[34] J.J.Erpenbeck. Nonlinear Theory of Unstable Two-Dimensional Detonation. *Phys.Fluids*, 13:2007–2026, 1970.

[35] Anne Bourlioux. *Numerical Study of Unstable Detonations, PhD Dissertation*. Princeton University, 1991.

[36] M.H.Lefebvre et al. The Influence of the Heat Capacity and Diluent on Detonation Structure. *Combustion and Flame*, 95:206–218, 1993.

[37] M.Dormal, J.C.Libouton, and P.VanTiggelen. *Acta Astronaut.*, 6:875, 1979.

[38] N.N.Yanenko. *The Method of Fractional Steps*. Springer-Verlag, 1971.

[39] E.S.Oran and J.P.Boris. *Numerical Simulation of Reactive Flow*. Elsevier Science Publishing, New York, 1987.

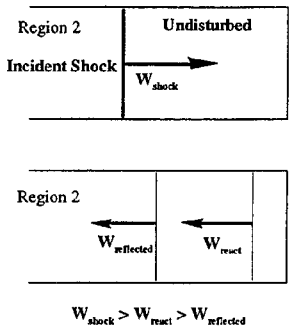

Figure 1: Schematic of the geometry used in the shock tube calculations. Top panel: incident shock of speed W_{shock} traveling to the right and reflected at the wall. Lower panel: the propagation of the reaction wave into region 2 in later time. Reactive wave will eventually catch up with the reflecting shock and become a transmitted detonation.

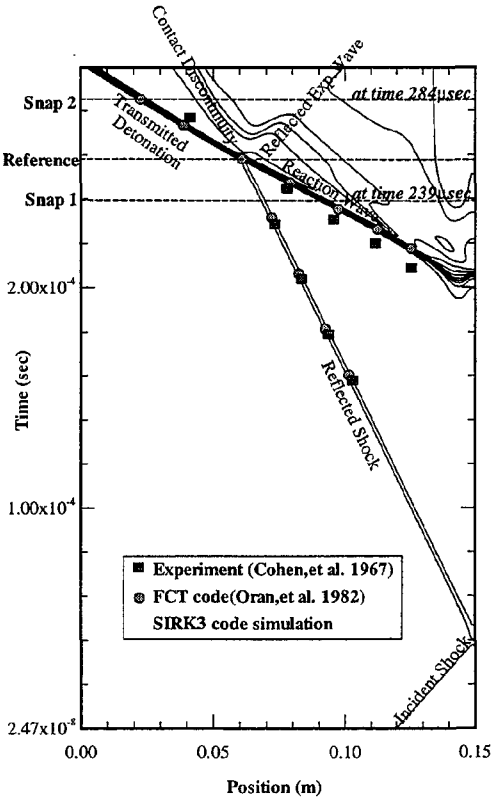

Figure 2: Calculated temperature contour, showing the position of the reflected shock front, reactive wave, transmitted detonation, contact discontinuity, and reflected expansion wave as a function of time. See Figure[3] for Snap1 and Figure[4] for Snap2. Wall is on the right side.

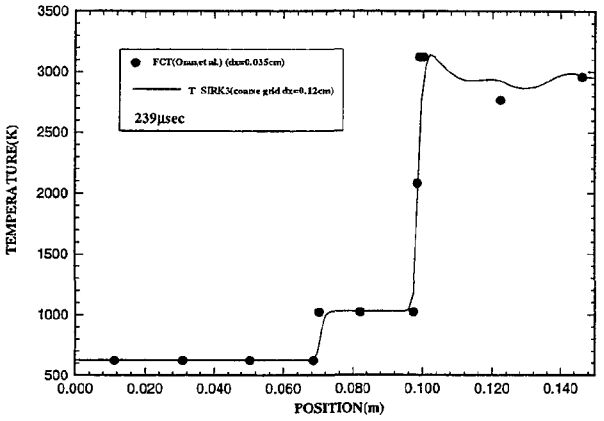

Figure 3: Snapshot1: calculated temperature profile at time before reacting wave catching up with reflected shock. Waves are traveling to the left.

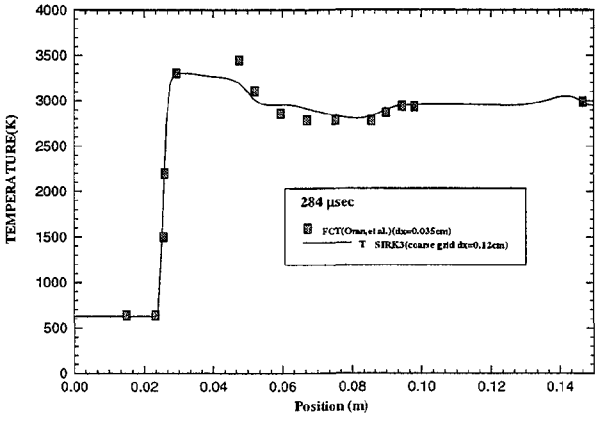

Figure 4: Snapshot2: calculated temperature profile at time the transmitted detonation, contact discontinuity, and reflected expansion wave are observed.

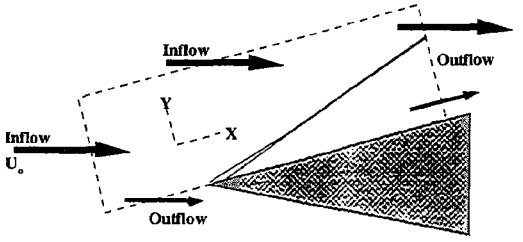

Figure 5: **Schematic of the computational domain attached to the wedge surface.**

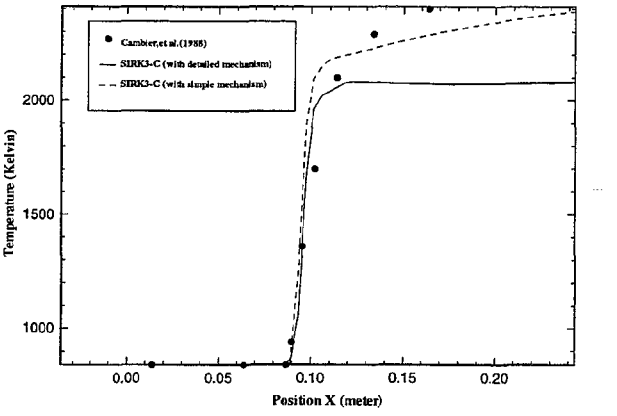

Figure 7: **Calculated temperature profile along the cut at grid row 32**

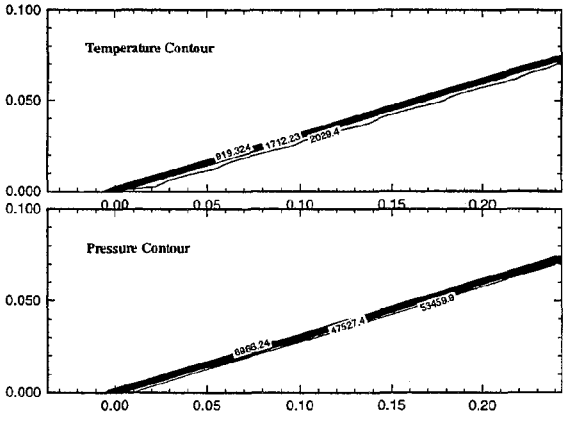

Figure 6: **Temperature and pressure contour for case in Table[3] on a 23° wedge.**

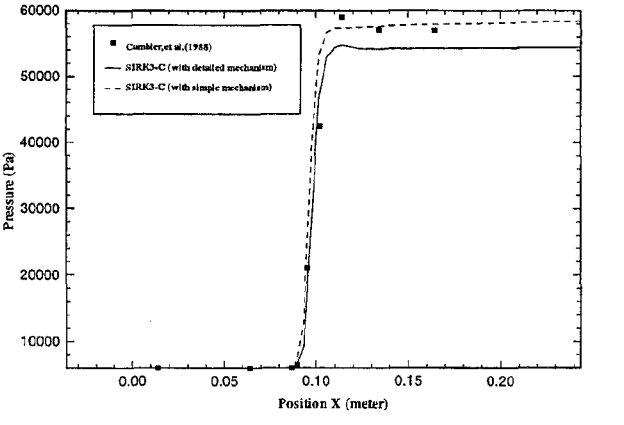

Figure 8: **Calculated pressure profile along the cut at grid row 32.**

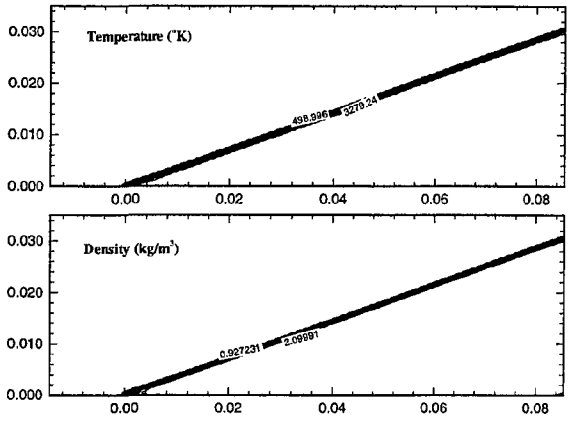

Figure 9: **Temperature and density contour for case in Table[4] on a 23° wedge in stoichiometric hydrogen-air mixture($H_2 : O_2 : N_2/2 : 1 : 3.76$ by moles)**

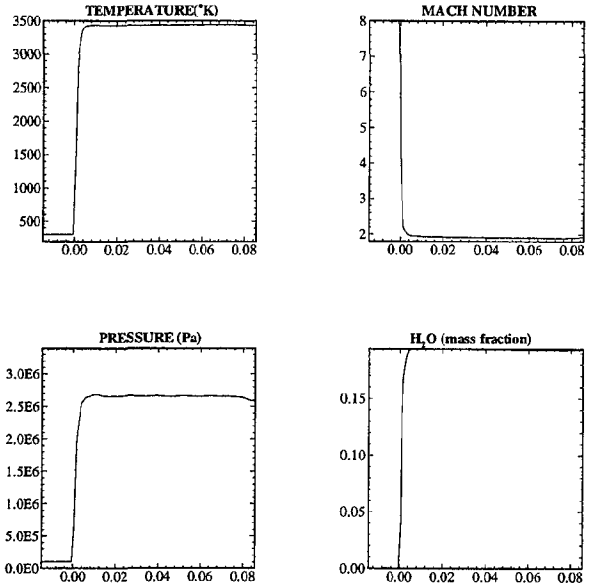

Figure 11: **Profiles of temperature, Mach number, pressure,and mass fraction of water along the x direction at $1.0mm$ above the wall from the simulation shown in Figures[9][10].**

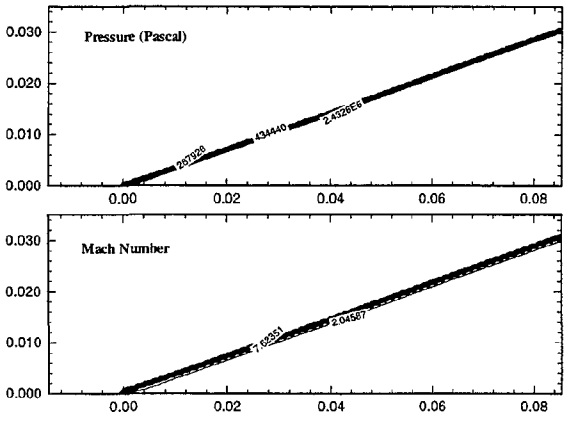

Figure 10: **Pressure and Mach number contour for case in Table[4] on a 23° wedge in stoichiometric hydrogen-air mixture($H_2 : O_2 : N_2/2 : 1 : 3.76$ by moles)**

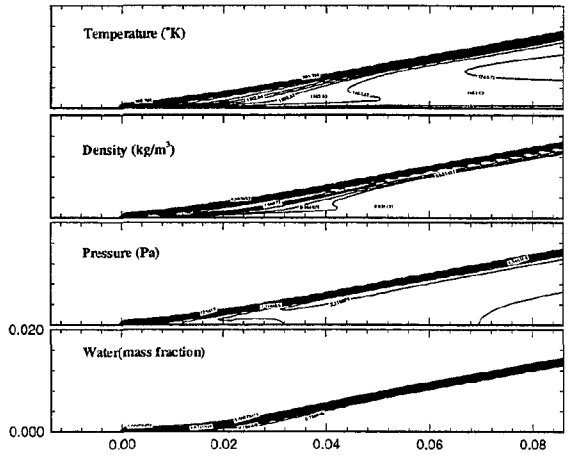

Figure 12: **A steady detonation structure on a 23° wedge in a 200 by 70 grid simulation.**

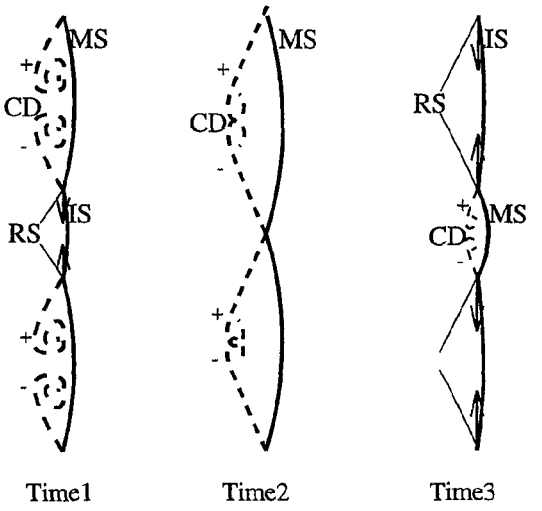

Figure 13: **Schematic of triple points movements: just before the triple points collision at Time1, at collision in Time2, and after the triple points collision at Time3. Roll-up vortices of opposite direction are found behind the Mach shocks(MS) while Reflected shocks(RS) are impinged on the Incident shock(IS) at triple points.**

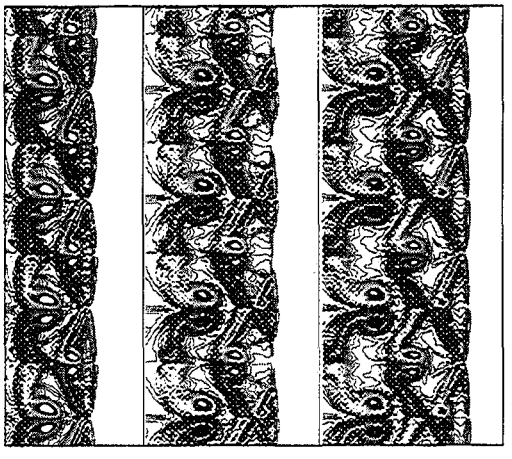

Figure 14: **Sequence of three snapshots of the flow field through a cell with vorticity.** $E^+ = 10; Q^+ = 50; f = 1.2$

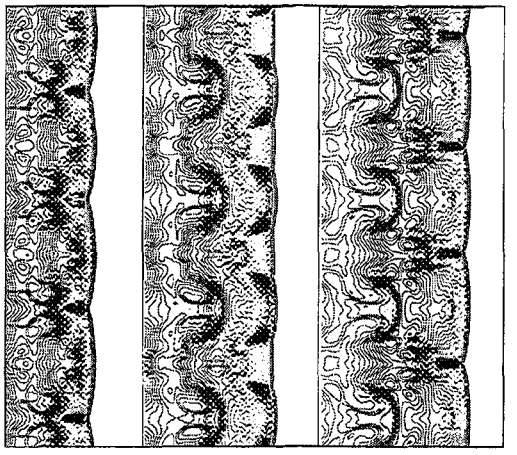

Figure 15: **Sequence of three snapshots of the flow field through a cell with density.** $E^+ = 10; Q^+ = 50; f = 1.2$

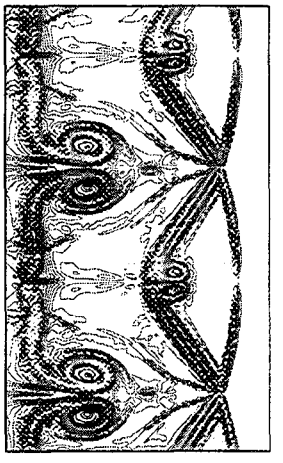

Figure 16: **Doubled grid result of vorticity field.** $E^+ = 10; Q^+ = 50; f = 1.2$

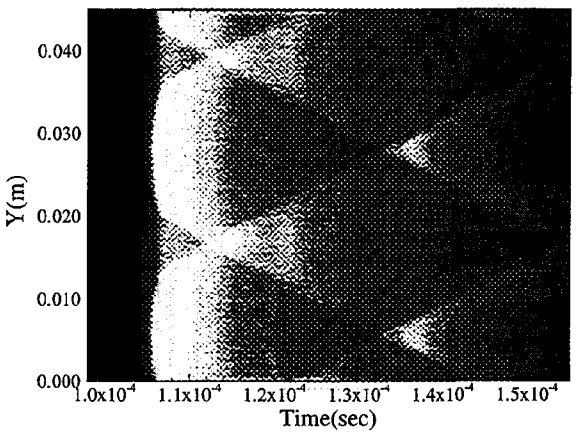

Figure 17: **Tracks of triple points on pressure contours in the Y-t plane**

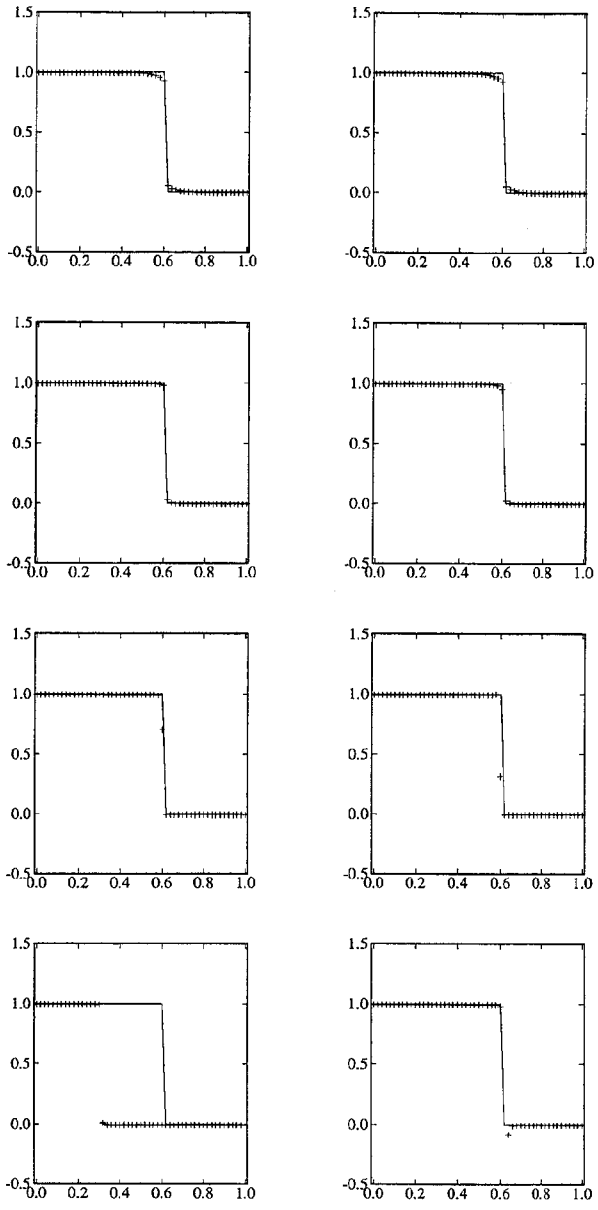

Figure 18: **Numerical results using (A) SIRK-3C with ENO-Roe-3 and (B) Time-Splitting with ENO-Roe-3/RK-3. The cell Damköhler numbers are $k\mu$ = 0, 0.15, 1.5, 15, increasing from top to bottom. -:true solution. +:computed solution.**

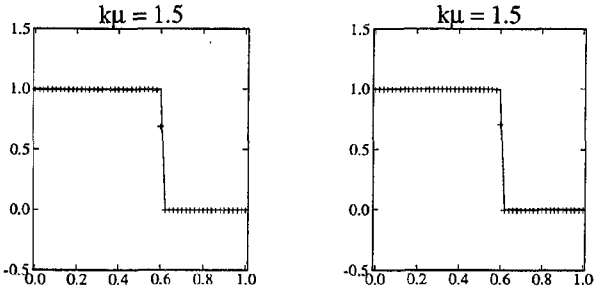

Figure 19: **Comparison of the two versions of the Semi-Implicit Runge-Kutta schemes at $k\mu = 1.5$: (A) fully iterative SIRK-3A, (B) Rosenbrock-type SIRK-3C; ENO-Roe-S-3 is the convective scheme used in both cases. -: exact solution. +: computed solution.**

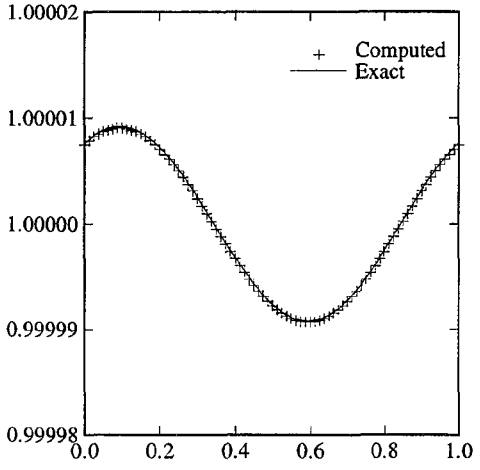

Figure 20: **Numerical result using SIRK-3C with third-order explicit upwind scheme shows no visible discrepancy in the propagation of a sinusoidal wave of length one at a moderate stiffness($\mathcal{D} = 30$). -:analytical solution at small ϵ. +:computed solution.**

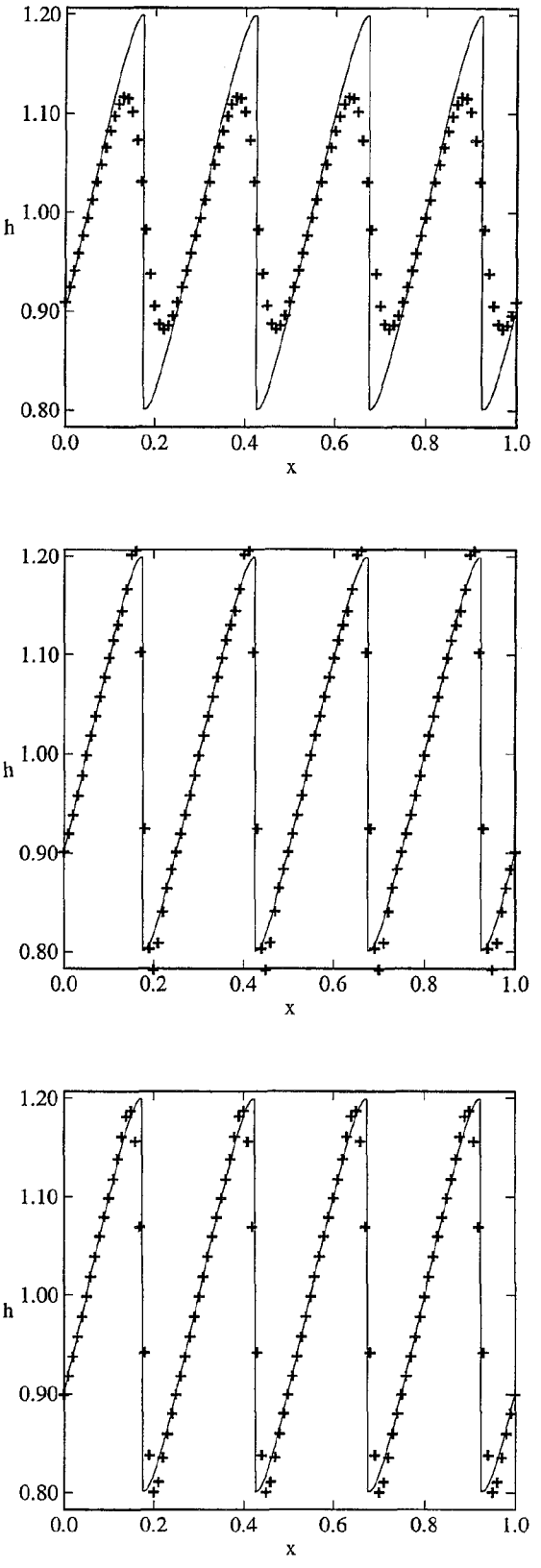

Figure 21: **Numerical results using Strang-Splitting, Second-order Splitting, and SIRK-3C from top to bottom. ($\mu = 10^8$, $t = 0.3$. -: exact solutions, +: numerical solutions)**

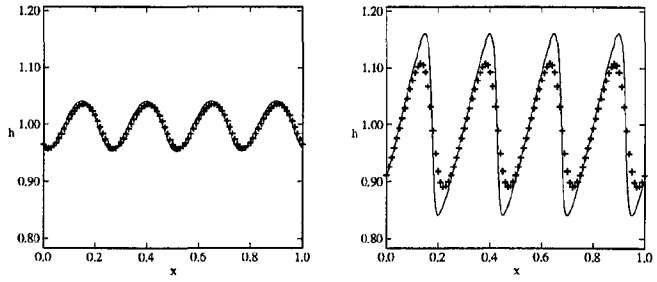

(A) (B)

Figure 22: **Strang-Splitting at varied stiffness: (a) μ = 100 and (b) μ = 1000 (t = 0.3. -: exact solutions, +: numerical solutions)**

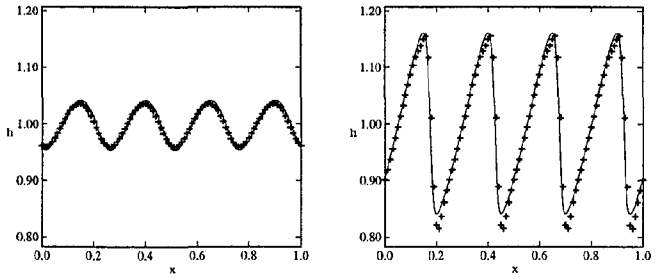

(A) (B)

Figure 23: **Second-order Splitting at varied stiffness: (a) μ = 100 and (b) μ = 1000 (t = 0.3. -: exact solutions, +: numerical solutions)**

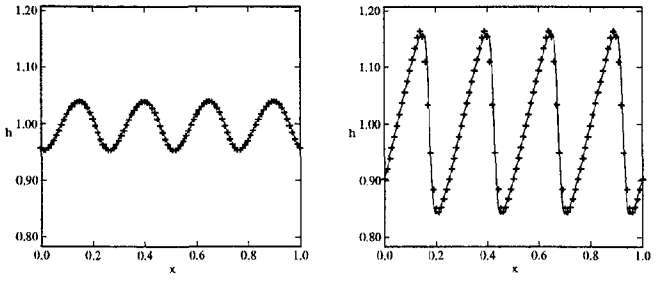

(A) (B)

Figure 24: **SIRK-3C at varied stiffness: (a) μ = 100 and (b) μ = 1000 (t = 0.3. -: exact solutions, +: numerical solutions)**